Journal of Power Sources 196 (2011) 4695–4704

Contents lists available at ScienceDirect

Journal of Power Sources

journal homepage: www.elsevier.com/locate/jpowsour

Analytical investigations of varying cross section microstructures on charge transfer in solid oxide fuel cell electrodes

George J. Nelson, Aldo A. Peracchio, Wilson K.S. Chiu*

HeteroFoaM Center, a DOE Energy Frontier Research Center, Department of Mechanical Engineering, University of Connecticut, 191 Auditorium Road, Storrs, CT 06269-3139, United States

ARTICLE INFO

Article history:
Received 8 November 2010
Received in revised form
17 December 2010
Accepted 21 December 2010
Available online 12 January 2011

Keywords:
Solid oxide fuel cell
Heterogeneous functional materials
Transport phenomena
Electrode microstructure

ABSTRACT

An extended surface modeling concept (electrochemical fin) is applied to charge transport within the SOFC electrode microstructure using an analytical modeling approach analogous to thermal fin analysis. This model is distinct from similar approaches applied to SOFC electrode microstructure in its application of a governing equation that allows for variable cross-section geometry. The model presented is capable of replicating experimentally observed electrode behavior inclusive of sensitivity to microstructural geometry, which stands in contrast to existing models that apply governing equations analogous to a constant cross-section thermal fin equation. Insights learned from this study include: the establishment of a suite of dimensionless parameters and performance metrics that can be applied to assess electrode microstructure, the definition of microstructure-related transport regimes relevant to electrode design, and correlations that allow performance predictions for electrodes that provide cell structural support. Of particular note, the variable cross-section modeling approach motivates the definition of a sintering quality parameter that quantifies the degree of constriction within the conducting network of the electrode, a phenomenon that exerts influence over electrode polarization. One-dimensional models are presented for electrochemical fins of several cross-sectional geometries with the ultimate goal of developing a general tool that enables the prompt performance evaluation of electrode microstructures. Such a tool would facilitate SOFC microstructural design by focusing more detailed modeling efforts on the most promising microstructures.

1. Introduction

The successful design and deployment of solid oxide fuel cells (SOFC) systems within a sustainable energy infrastructure is an inherently multi-scale problem that may benefit from the deliberate design of fuel cell components at the nano- and micro-scales [1]. A variety of modeling approaches exist for the detailed exploration of electrochemistry and transport at these scales. While detailed microstructural models serve as powerful design tools, the associated high computational costs suggest intensive modeling is best reserved for the optimization of promising microstructural design candidates. Thus, the development of simplified models that can effectively screen candidate designs is warranted. One such approach involves the application of extended surface (fin) models to the description of charge transport within SOFC components. Several existing models apply equations for the description of charge transport within SOFC electrodes that are similar to the governing equation for a constant cross-section thermal fin [2–8]. Other works apply extended surfaces that are modeled as a means of replicating electrode behavior. These approaches include analytical [3,8,9] and numerical models [2,4,5,7,8].

An early example of an SOFC electrode model that uses a governing equation comparable to the thermal fin equation can be found in studies of electrode resistance performed by Kenjo et al. [9,10]. The analysis presented by Kenjo et al. [9] applied a thin film model to describe electrode performance that followed models of electrode operation in liquid electrolyte fuel cells. This model treated the electrolyte phase as a thin film lining the pores of the electrode and was cast in terms of a local polarization with charge transfer resistance and microstructural geometry lumped into a single interfacial impedance parameter. Microstructural geometry was introduced to the model through the pore radius, which represents an inversion of more recent approaches that focus on the microstructure of solid phases. While details of microstructural influence were not provided, Kenjo et al. did provide some key insights on electrode operation including demonstration of: electrode types for which the thin film model is insufficient (e.g., poorly sintered electrodes), limits for polarization resistance based on electrode thickness, and

* Corresponding author at: University of Connecticut, Department of Mechanical Engineering, 191 Auditorium Road, Unit 3139, Storrs, CT 06269-3139, United States. Tel.: +1 860 486 3647; fax: +1 860 486 5088.
E-mail address: wchiu@engr.uconn.edu (W.K.S. Chiu).

0378-7753/$ – see front matter © 2011 Elsevier B.V. All rights reserved.
doi:10.1016/j.jpowsour.2010.12.103

Nomenclature

A	area (m^2)
a	slope of variable cross-section fin profile
i	current (A)
L	length of fin segment (m)
L_{act}	electrode active length (m)
L_f	total fin length or electrode thickness (m)
P	perimeter of constant cross-section fin (m)
R	area specific resistance ($\Omega\,m^2$)
r	fin radius (m)
SQ	sintering quality
V	voltage (V)

Greek symbols

ε_f	fin effectiveness
η_f	fin efficiency
ρ	resistivity ($\Omega\,m$)
σ	conductivity ($S\,m^{-1}$)
φ	potential difference (V)

Subscripts

b	quantity evaluated at fin base
c	quantity related to fin cross-section
ct	charge transfer
el	electronic
io	ionic
pol	polarization
s	quantity related to fin surface
t	quantity evaluated at fin tip

the benefits of increased electrode thickness with respect to reducing polarization resistance.

Electrode charge transport models following the work of Kenjo et al. largely shifted focus to the analysis of charge transport in the solid phases [2–8,11], foregoing a strict thin film interpretation and applying comparable equations to extended surfaces. Tanner et al. [2] presented an extended surface model of an SOFC electrode that focused on solid state charge transport within the electrolyte phase. In contrast to the work of Kenjo et al., this model treated the electrolyte as the extended surface and the electrocatalyst as thin film coating the electrolyte. A charge transfer resistance governed transport between the electrolyte and electrocatalyst phases. A governing equation similar to the thermal fin equation was developed assuming a constant potential within the electrocatalyst layer, and the general solution developed bears a strong resemblance to general solutions of the thermal fin problem [2]. Ultimately, the model developed enabled consideration of the influence of electrode porosity and the thickness of the electrode and electrolyte regions. As in the work of Kenjo et al., thicker electrodes were shown to be beneficial from the standpoint of reducing effective charge transfer resistance. The model presented also addressed the influence of electrochemically active regions at the electrolyte interface. Furthermore, using a numerical solution, the role of charge transfer resistance and two-dimensional transport were explored. In addition to the work of Tanner et al. the extended surface concept has been applied to describe charge transport within SOFC cathodes [12] and in the development of equivalent circuit models for MIEC electrodes [13].

Costamagna et al. [3,11] presented a version of the extended surface model in which the potential of the electronic conducting phase was allowed to vary. Using a linearized form of the Butler–Volmer equation to describe surface exchange and several dimensionless parameters and variables, they solved an ordinary differential equation comparable to the fin equation that ultimately describes the overpotential within an SOFC electrode composed of packed spheres. Performance in terms of polarization resistance was explored as a function of electrode thickness and composition in relation to percolation thresholds and particle sizes. Optimum compositions were found near the percolation thresholds for the electronic conducting phase. The work of Costamagna et al. is one example of an array of packed sphere models that apply percolation theory to study the impact of microstructure on SOFC transport phenomena [4–8,14–16]. Such models typically require either the application of effective conductivities [4,5,14] or the numerical solution of random resistance networks [7,8,15,16]. Of particular note, the work of Sunde's drew upon percolation theory and the numerical solution of three-dimensional resistor networks to simulate the conductivity and polarization resistance of SOFC electrodes as functions of electrode composition [7,8]. The general model formulation and dimensionless parameters applied in Sunde's exploration of polarization resistance are comparable to those applied later by Costamagna et al. [3,8].

In addition to the solution of resistor networks, several other numerical techniques have been applied to describe more detailed transport than allowed by the simplified cases addressed by analytical models. Cannarozzo et al. [5] revisit the work of Costamagna et al. using a more detailed, composition dependent form of the Butler–Volmer equation. The equations they established were solved using a collocation method, and the resulting model demonstrated trade-offs that exist between activation and concentration losses that can be linked to particle size. Tanner et al. [2] used a two-dimensional finite difference method to establish more detailed potential distributions within an extended YSZ structure that served as a benchmark for their simplified one-dimensional model. Fleig and Maier [12] solved a similar problem for charge transport within the cathode using finite element analysis to characterize charge transport in structures resembling an array of pin fins. This model allowed for the establishment of cathode operational regimes that distinguished the level of electrochemical activity within the structure. Finally, Zhu and Kee [4] developed a detailed set of differential algebraic equations (DAEs) describing mass, charge and energy transport within the electrodes and electrolyte of an SOFC. This system of equations was solved using a DAE solution software. Trade-offs between activation and concentration losses were demonstrated to occur based on varying particle sizes, and polarization was shown to primarily occur in the ionic conducting phase. The electronic conducting phase was found to have almost constant overpotential.

This article addresses the application of the extended surface modeling concept to charge transport within SOFC electrodes using an analytical modeling approach that focuses on the solid, ionic conducting phase in the electrode. While this model varies from the thin film approach in terms of the phase of interest, parallels between the approaches are strong enough to warrant cognizance of thin film model critiques that may apply. Most notably thin film models have been considered to not fully account for several composition related phenomena that have been witnessed in electrode experiments [6]. The present work attempts to address one such issue, connectivity of the ionic conducting phase, by developing an extended surface model that allows for variable cross-section geometry. When applied to periodic structures, this allowance enables varying degrees of connectedness. The model presented also demonstrates sensitivity to microstructural geometric details without a reliance on effective conductivity parameters. This sensitivity stands in contrast to many existing models, even several based on percolation theory, that apply governing equations analogous to constant cross-section thermal

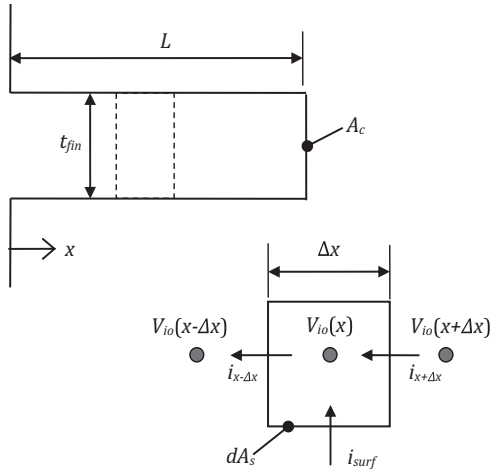

Fig. 1. Basic geometry of a constant cross-section electrochemical fin following Tanner et al. [2].

fin equations [3,5–9]. Such approaches may neglect the influence that microstructural geometry plays in electrode performance because they do not fully account for variations in geometry within their fundamental equations. The enhanced sensitivity in the models developed is achieved by extending constant cross-section modeling approaches to variable cross-section equations. One-dimensional models are developed for electrochemical fins of several cross-sectional geometries with the ultimate goal of developing a general tool that enables the prompt performance evaluation of electrode microstructures. Such a tool would facilitate SOFC microstructural design by focusing more detailed modeling efforts on the most promising microstructures.

2. Model formulation

2.1. Analytical models

The analytical model presented is developed for an extended surface of ion conducting material subject to charge transfer. The governing equation for this system is referred to herein as the fin equation. Following the work of Tanner et al. [2] a basic case for the fin equation was developed using the geometry shown in Fig. 1. Arrows indicate flux of oxygen ions, and the currents flowing across each boundary are defined in Eqs. (1)–(3). Several key simplifying assumptions are applied in this derivation. Most notably, transport is assumed to be one-dimensional across the thickness of the electrode. Gas transport is assumed to be fast, such that reactant composition does not vary along the surface of the geometry considered. This condition allows for linear treatment of the Butler–Volmer equation in the form of a single charge transfer resistance parameter. Finally, two assumptions are applied regarding the physics of charge transport. First, charge transport is assumed to be primarily ionic with constant potential assumed in the electronic conducting phase. This assumption may be relaxed, as done in studies based on percolation theory [3–5]. However, it is interesting to note that in the event that $\rho_{io} \gg \rho_{el}$, effective conductivities applied in such models [3] will be dominated by the ionic conducting phase. Furthermore, the detailed modeling results of Zhu and Kee [4] predict negligible variation in electronic potentials across the substantial portions of the electrodes. Second, the effects of space charge regions near grain boundaries on ionic transport are neglected in the present work. These space charge regions may exert influence on electrode performance at lower temperatures or for electrodes composed of smaller particles (grain size less than 1 μm) [17], and may be considered in subsequent works.

$$i_{x+\Delta x} = -\sigma_{io} A_c \frac{V_{io}(x) - V_{io}(x+\Delta x)}{\Delta x} \tag{1}$$

$$i_{x-\Delta x} = -\sigma_{io} A_c \frac{V_{io}(x-\Delta x) - V_{io}(x)}{\Delta x} \tag{2}$$

$$i_{surf} = dA_s \frac{1}{R_{ct}} [\Delta V^{eq} - (V_{io}(x) - V_{el}(x))] \tag{3}$$

Here, ΔV^{eq} is defined as the equilibrium potential for the electrode [5]. If $V_{el}(x)$ is held constant across the electrode thickness a reference potential can be defined as shown in Eq. (4). Assuming a constant cross-section the surface current can be expressed in terms of this reference potential.

$$V^0 = \Delta V^{eq} + V_{el} \tag{4}$$

$$i_{surf} = -P\Delta x \frac{1}{R_{ct}} [V_{io}(x) - V^0] \tag{5}$$

To develop the ordinary differential equation (ODE) for the basic case, a charge balance is established similar to the form applied by Tanner et al. [2]. As the width of the differential element approaches zero this balance becomes the ODE shown in Eq. (7).

$$-\sigma_{io} A_c \frac{V_{io}(x) - V_{io}(x+\Delta x)}{\Delta x} - P\Delta x \frac{1}{R_{ct}} \left[V_{io}(x) - V^0\right] = -\sigma_{io} A_c \frac{V_{io}(x-\Delta x) - V_{io}(x)}{\Delta x} \tag{6}$$

$$-\sigma_{io} A_c \frac{d^2 V_{io}(x)}{dx^2} + P \frac{1}{R_{ct}} V_{io}(x) = P \frac{1}{R_{ct}} V^0 \tag{7}$$

To fully leverage the fin analogy, a potential difference is defined and the equation is recast in the standard fin equation form. This potential difference, shown in Eq. (8), is analogous to expressing the fin temperature distribution of a find undergoing heat transfer in terms of the difference between the fin temperature and the base temperature.

$$\varphi(x) = V_{io}(x) - V^0 \tag{8}$$

$$\frac{d^2\varphi}{dx^2} - \left(\frac{P}{A_c}\right) \frac{1}{\sigma_{io} R_{ct}} \varphi = 0 \tag{9}$$

The term separated by parentheses in Eq. (9) is highlighted as a geometric parameter for the fin. Specifically, it is the ratio of the perimeter to the cross-sectional area that is commonly encountered in thermal fin analysis. A key distinction can be drawn between this form of the equation and the lumped parameter approach applied by Kenjo et al. [9]. Specifically, the form shown in Eq. (9) allows for separating microstructural parameters and physical constants associated with charge transport. The general solution takes the form shown in Eq. (10), with the constant m defined in Eq. (11). The constants that complete the particular solution will be discussed shortly.

$$\varphi(x) = C_1 \exp(mx) - C_2 \exp(-mx) \tag{10}$$

$$m = \sqrt{\frac{P}{A_c} \frac{1}{\sigma_{io} R_{ct}}} \tag{11}$$

As noted, equations following the form of Eq. (9) have been explored in electrode models based on percolation theory [3,5–8,11]. However, by implementing constant cross-section equations like Eq. (9) these works tacitly neglect the role that cross-sectional area and its variation within the microstructure play in the equation governing charge transport. In the present work a variable cross-section form of this governing equation and its solution are presented for geometries based on a conical frustum building block. This geometry is shown in its basic a periodic forms in Fig. 2. For

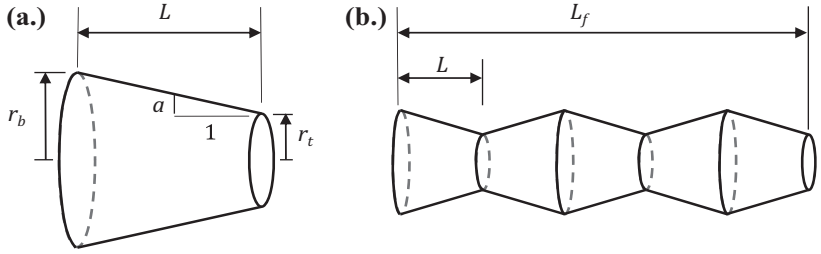

Fig. 2. Variable cross-section pin fin structures with geometry of (a) a conical frustum and (b) a periodic structure composed of iterated conical frusta.

the case of a variable cross-section fin the governing ODE, Eq. (7), can be recast in the general form of Eq. (12). The general solution of Eq. (12) for the conical geometry shown in Fig. 2a is given in Eq. (13), where I_1 and K_1 are first order modified Bessel's functions of the first and second kind, respectively. The relevant parameters for Eq. (13) are defined in Eqs. (14) and (15).

$$\frac{d^2\varphi}{dx^2} + \frac{1}{A_c}\frac{dA_c}{dx}\frac{d\varphi}{dx} - \frac{1}{\sigma_{io}R_{ct}A_c}\frac{dA_s}{dx}\varphi = 0 \tag{12}$$

$$\varphi[r(x)] = \frac{1}{\sqrt{r(x)}}\left[C_1 I_1(\beta\sqrt{r(x)}) + C_2 K_1(\beta\sqrt{r(x)})\right] \tag{13}$$

$$r(x) = r_b - ax \tag{14}$$

$$\beta = \sqrt{\frac{8}{\sigma_{io}R_{ct}}\frac{\sqrt{1+a^2}}{a^2}} \tag{15}$$

For non-periodic geometries (Figs. 1 and 2a) the constants C_1 and C_2 in Eqs. (10) and (13) can be readily defined for an array of boundary conditions. In the present work a constant potential, φ_b, is fixed at the base of the structure, and active charge transfer is assumed at the tip of the structure. This latter boundary condition is chosen in lieu of the more common insulated tip condition because the assumption of an insulated tip precludes the possibility of charge being consumed at the end of the fin structure. For a short percolating structure connected to the electrolyte like those illustrated by Sunde [8] it is possible that charge may be transported to and consumed at the tip of the structure. Removing these structures from consideration is not desired. Furthermore, for a sufficiently thick electrode (i.e., a long fin) charge will be completely consumed along the fin perimeter and does not reach the tip of the fin. Thus for sufficiently long fins the active tip will be effectively insulated, and implementing an active tip condition is considered to mimic electrochemically active, connected ion conducting structures that do not extend across the full thickness of the electrode, like those illustrated by Sunde [8]. The constants for the particular solution of Eq. (7) corresponding to these boundary conditions are shown in Eqs. (16) and (17). Similarly, the constants for the particular solution of Eq. (12) subject to these conditions are given in Eqs. (18) and (19).

$$C_1 = \frac{\varphi_b \exp(-mL_f)((1/R_{ct}) - \sigma_{io}m)}{((1/R_{ct}) - \sigma_{io}m)\exp(-mL_f) - \left((1/R_{ct}) + \sigma_{io}m\right)\exp(mL_f)} \tag{16}$$

$$C_2 = \varphi_b - C_1 \tag{17}$$

$$C_1 = \frac{\varphi_b\sqrt{r_b}[r_t^{-1/2}K_1(\beta\sqrt{r_t}) - (\beta/2)K_0(\beta\sqrt{r_t})]}{I_1(\beta\sqrt{r_b})[r_t^{-1/2}K_1(\beta\sqrt{r_t}) - (\beta/2)K_0(\beta\sqrt{r_t})] - K_1(\beta\sqrt{r_b})[r_t^{-1/2}I_1(\beta\sqrt{r_t}) - (\beta/2)I_0(\beta\sqrt{r_t})]} \tag{18}$$

$$C_2 = \frac{\varphi_b\sqrt{r_b} - C_1 I_1(\beta\sqrt{r_b})}{K_1(\beta\sqrt{r_b})} \tag{19}$$

For periodic structures (Fig. 2b), the definition of the appropriate constants is not as straightforward. However, modeling of such structures can be achieved by recognizing that each of the n segments comprising the structure obeys the general solution shown in Eq. (13). A system of $2n$ equations can then be established by applying the base and tip boundary conditions and invoking constraints based on equipotential and current conservation at interior segment boundaries (at $x = 2L, 3L, \ldots, (n-1)L$). Subsequent solution of this system of equations yields the values of the constants for the n particular solutions.

Limiting cases for the one-dimensional transport model presented above arise primarily for poorly sintered electrodes and electrodes composed of small particles. Poorly sintered geometries with small interparticle neck sizes may exhibit multi-dimensional potential distributions. However, these variations are expected to be small compared to bulk potential drops for electrodes with thicknesses greater than a few particle sizes. Thus, thin poorly sintered electrodes may be considered a limiting case for the model presented. As noted, space charge effects that may exert greater influence in electrodes composed of small particles and in lower temperature operation also present a limiting case for the applicability of the current form of the electrochemical fin model. Incorporation of these effects may be addressed in subsequent works.

2.2. Microstructural and performance parameters

Considering the complicated expressions involved in direct implementation of the analytical solutions above, it is desirable to develop some basic parameters that can be used to describe the microstructure and predict the performance of an SOFC electrode. Such parameters can be defined by first establishing a dimensionless form of Eq. (12) (shown in Eq. (20)) using a normalized potential, $\varphi^* = \varphi/\varphi_b$, normalized length, $x^* = x/L_f$, and two normalized area terms, $A_s^* = A_s/A_{c,b}$ and $A_c^* = A_c/A_{c,b}$.

$$\frac{d^2\varphi^*}{dx^{*2}} + \frac{1}{A_c^*}\frac{dA_c^*}{dx^*}\frac{d\varphi^*}{dx^*} - \frac{L_f}{\sigma_{io}R_{ct}A_c^*}\frac{dA_s^*}{dx^*}\varphi^* = 0 \tag{20}$$

The first parameter developed from Eq. (20) is a resistivity ratio (ρ_{io}/ρ_{ct}) based on the third term on the left-hand side. Similar forms of this term have been previously defined by Sunde and Costamagna et al. [3,6,8]. These existing forms were defined based on the triple-phase boundary (TPB) concentration in the electrode, instead of using a direct relation to the microstructural cross-section and surface areas applied in Eqs. (12) and (20) (e.g., $(1/A_c)dA_s/dx$). Deference is given to this latter analytical form in the present work to minimize the use of empirical factors in the model. As indicated in Eq. (21) the resistivity ratio compares the ionic resistivity of the electrode and a charge transfer resistivity that depends on the electrode thickness, the fin cross-sectional area and variation in the fin surface area. This parameter is derived directly in producing the dimensionless form of the governing equation. As an operator on

the normalized potential term, it represents a dimensionless surface charge transfer coefficient that quantifies the balance between the rate of conductive charge transfer through the solid structure to the chemically active surface and the rate of charge transfer from the chemically active surface. The ionic conductivity and cross-sectional area terms reflect the influence of conduction within the solid. Reducing either of these factors increases the influence of conductive charge transfer. The charge transfer resistance and change in surface area reflect the role of surface charge transfer. Increasing the former reduces the rate of charge transfer from the active surface, while increasing the latter provides gains in charge transfer relative to conduction. The length dependence seen in the resistivity ratio reflects the increased surface charge transfer resulting from further extension of the active surface. For the conical structures shown in Fig. 2 this resistivity ratio can be defined by taking the average of the area terms over the segment length L, as shown in Eq. (22).

$$\frac{\rho_{io}}{\rho_{ct}} = \frac{L_f^2}{\sigma_{io} R_{ct}} \frac{1}{A_c} \frac{dA_s}{dx} \tag{21}$$

$$\frac{\rho_{io}}{\rho_{ct}} = \frac{L_f^2}{\sigma_{io} R_{ct}} \left(\frac{1}{L} \int_0^L \frac{1}{A_c} \frac{dA_s}{dx} dx \right) = -2 \frac{L_f^2}{L \sigma_{io} R_{ct}} \frac{\sqrt{1+a^2}}{a} \ln\left(\frac{r_t}{r_b}\right) \tag{22}$$

The introduction of the middle term on the left-hand side of Eqs. (12) and (20) accounts for the additional influence variation in cross-sectional geometry exerts on performance. This influence can be described using a parameter that is herein defined as the sintering quality of the electrode microstructure, SQ. A poorly sintered geometry is considered to have a relatively small neck radius compared to the particle radius [9,17], which would result in a high value for the coefficient $(1/A_c)dA_c/dx$. Thus the sintering quality is defined as the inverse of this coefficient to reflect the appropriate dependence on neck radius, Eq. (23). A constant cross-section geometry would be considered as "perfectly sintered" and would have an infinite sintering quality. The sintering quality quantifies the role that constrictions within the sintered geometry play in increasing the ohmic losses within the electrode and can be readily cast in terms of the conical geometries considered following the approach used for the resistivity ratio, as shown in Eq. (24).

$$SQ = \left[\frac{L_f}{A_c} \frac{dA_c}{dx} \right]^{-1} \tag{23}$$

$$SQ = \left[\frac{L_f}{L} \int_0^L \frac{1}{A_c} \frac{dA_c}{dx} dx \right]^{-1} = \left[-2 \frac{L_f}{L} \ln\left(\frac{r_t}{r_b}\right) \right]^{-1} \tag{24}$$

The resistivity ratio and sintering quality provide a basis for describing SOFC electrodes using microstructural geometry and basic properties of the electrode, the ionic conductivity and charge transfer resistance. However, additional performance metrics are needed for the resistivity ratio and sintering quality to properly facilitate electrode analysis and design. These metrics can be drawn from existing SOFC literature and by adapting parameters from thermal fin analysis. Dimensionless currents have been applied as boundary conditions in the analysis of composite electrodes [3,6]. In the present work, the analytical solutions developed have been used to define a dimensionless base current that describes the total charge transferred across the electrode–electrolyte interface at the base of the electrochemical fin. The current can be expressed in terms of the potential, φ, following Eq. (25), given in a general form for brevity.

$$\left.\frac{d\varphi^*}{dx^*}\right|_{x^*=0} = \frac{L_f}{\varphi_b} \left.\frac{d\varphi}{dx}\right|_{x=0} \tag{25}$$

Following the thermal fin example the efficiency, η_f, and the effectiveness, ε_f, can be defined for the electrochemical fin model according to Eqs. (26) and (27). Here, A_f represents the total surface area of the fin, including the sides and tip. For the electrochemical case the efficiency compares the total current conducted by the fin to the ideal current that would be conducted by a constant voltage fin held at the base voltage, φ_b. This metric allows for evaluation of the conductive resistance for a given geometry, with a reduced efficiency indicating greater ohmic losses attributed to microstructural geometry. A similar parameter was introduced by Costamagna et al. [3], but was referred to as an effectiveness factor. The effectiveness defined in the present work compares the total current conducted by the fin to the current that would be conducted across an unmodified surface. This metric essentially determines whether a particular structure produces a significant impact when added to an electrolyte surface. The effectiveness accounts for both the surface charge transfer gained by adding the fin and the conductive resistance within the fin.

$$\eta_f = \frac{i_{tot}}{(1/R_{ct}) A_f \varphi_b} \tag{26}$$

$$\varepsilon_f = \frac{i_{tot}}{(1/R_{ct}) A_b \varphi_b} \tag{27}$$

A final performance metric applied in the analysis of SOFC electrodes is the polarization resistance, R_{pol}. This resistance is defined as the total current density flowing across the electrode–electrolyte interface divided by the potential at the same interface [9]. Inspection of Eq. (27) reveals that the polarization resistance can be expressed in terms of the effectiveness.

$$R_{pol} = \frac{R_{ct}}{\varepsilon_f} \tag{28}$$

In the present work the polarization resistance is used to compare predictions made by the electrochemical fin models to experimental measurements of the polarization resistance made by Kenjo et al. [9]. In further analyses, deference is given to the non-dimensional metrics defined above and this resistance is not applied. However, noting that the dimensionless base current can be cast in terms of the effectiveness (Eq. (29)) it can be seen that the dimensionless base current and the polarization resistance are inversely proportional. This relation may serve as a useful point of reference for those better acquainted with the polarization resistance.

$$\left.\frac{d\varphi^*}{dx^*}\right|_{x^*=0} = \frac{\varepsilon_f L_f}{\sigma_{io} R_{ct}} \Rightarrow \left.\frac{d\varphi^*}{dx^*}\right|_{x^*=0} \propto \frac{1}{R_{pol}} \tag{29}$$

The analytical models, dimensionless parameters and performance metrics outlined above provide a simplified means of rapidly assessing the impact of electrode microstructure on SOFC performance. Among the assumptions applied it should be noted that the influence of space charge and multidimensional transport require further consideration. This is especially the case for poorly sintered microstructures [17]. As noted, the incorporation of such effects will be pursued in subsequent works.

3. Results and discussion

3.1. Comparison to experiments

The predictive capabilities of the analytical model developed for SOFC microstructures were initially tested in comparison to experimental data published by Kenjo et al. for electrodes of varying

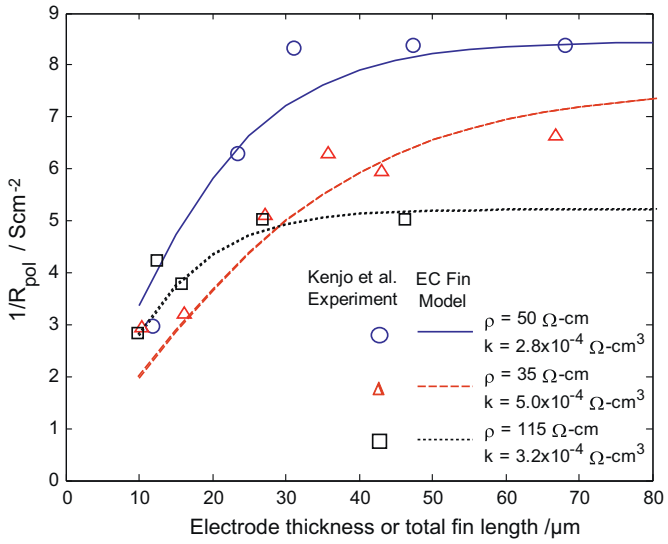

Fig. 3. Comparison of constant cross-section electrochemical fin model to experimental results from Kenjo et al. [9]; the fin radius was set to match the lumped parameter *k*. Consideration of the perimeter to cross-sectional area ratio in a constant cross-section model presents an improvement over lumped charge transfer parameters.

compositions (mixtures of erbia-doped bismuth oxide and platinum), resistivities and charge transfer characteristics [9]. This comparison is shown in Fig. 3 for the case of an electrode simulated with a constant cross-section cylindrical electrochemical fin model. It is clear that the model is capable of predicting the behavior of these well-sintered electrodes. The model presented allows for the incorporation of microstructural influence through the geometry of the extended surface. In the constant cross-section case this influence can be dictated by the ratio of the fin perimeter to cross-sectional area (P/A_c), a common metric seen in thermal fin analysis. To separate this influence from the lumped parameter used by Kenjo et al., a fixed charge transfer resistance of $0.6\,\Omega\,cm^{-2}$, and the radius of the cylindrical fin was modified to produce the appropriate lumped parameter value. While the constant cross-section model can be seen to compare well with the experimental data of Kenjo et al., it should be noted that these results still rely on modifying the geometry to match an empirical fitting parameter. Thus the agreement is achieved, demonstrating that the model is capable of predicting the performance of electrochemical fins with constant cross section.

Further exploration of the electrochemical fin approach can be achieved by comparing model predictions to electrode experiments shown in Fig. 4. Here electrodes noted by Kenjo et al. as well sintered are simulated using the constant and variable cross-section electrochemical fin approach, and electrodes noted as poorly sintered are simulated using only a variable cross-section model. The variable cross-section cases are simulated using periodic structures composed of conical frusta (Fig. 2b). All cases examined apply a base radius value of 2 μm, which for the constant cross-section case provides a strong match to the experimental data. The well sintered variable cross-section case applies a slightly smaller tip radius of 1.75 μm for each conical unit, and the poorly sintered cases apply tip radii of 0.2 μm and 0.125 μm. As with the cases shown in Fig. 3, each case demonstrates the capability of the electrochemical fin approach to account for the influence of microstructure on electrode performance. For the variable cross-section case, this influence is accounted for in both the charge transfer and ionic transport terms of the governing equation (Eq. (12)). However, limited microstructural data was made available by Kenjo et al. for the electrodes tested. More detailed investigations of SOFC electrode microstructure are needed to verify these predictions, but with the advent of advanced microstructural characterization techniques such as X-ray computed tomography (XCT) and focused ion beam-scanning electron microscopy (FIB-SEM) such direct verification against real microstructures is possible [18–22].

While the direct experimental comparisons of Fig. 4 are primarily qualitative, several key insights come to light from inspection of the results. First and foremost it can be clearly seen that more constricted, poorly sintered electrodes can be described by analytical models that allow for consideration of cross-sectional variation within the equation governing charge transport. The accounting for increased ohmic losses related to the higher degree of constriction within the microstructure enables the model to produce the "thickness effect" seen for electrodes that could not be discerned by

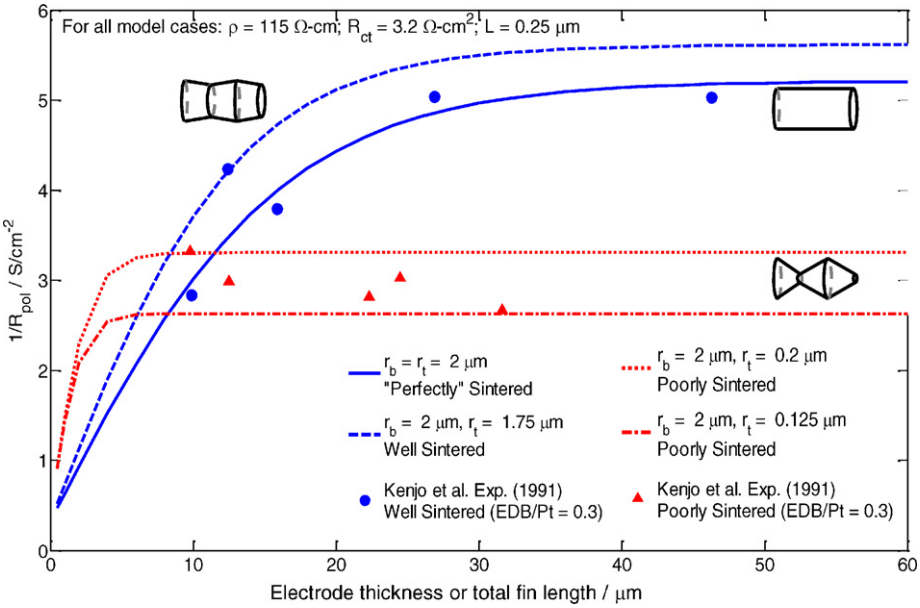

Fig. 4. Comparison of constant and variable cross-section electrochemical fin models to experimental results from Kenjo et al. [9] for well sintered and poorly sintered electrodes; fin geometries with little to no variation in cross-section represent well sintered structures while fins with drastic variations represent poorly sintered structures. For poorly sintered structures the agreement in behavior is seen as strictly qualitative.

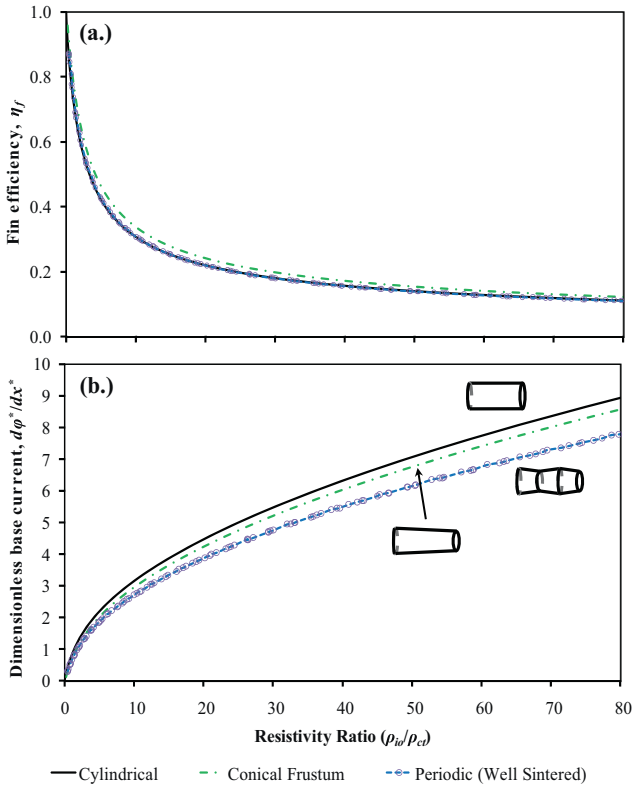

Fig. 5. Fin efficiency (a) and dimensionless base current (b) as functions of resistivity ratio for the geometries investigated (r_b = 2 μm for all cases, r_t = 1.75 μm for conical and periodic fins); while surface area gains may increase charge transfer a trade-off exists in balancing ohmic losses incurred by constrictions in the microstructure. The efficiency indicates well sintered geometries exhibit ohmic loss comparable to constant cross-section model predictions. However, overall polarization may show significant differences, as indicated by the dimensionless base current.

the constant cross-section thin-film model [9]. Secondly, the separation of charge transfer and microstructural effects achieved in the perimeter to cross-sectional area ratio applied in the cylindrical case is built upon by the further distinction of microstructural influence in the variable cross-section cases and motivates the development of parameters that address ohmic losses within the microstructure. Such parameters should be able to describe gains achieved by increasing active surface area, as seen in the well-sintered case, and losses caused by microstructural constrictions that detract from performance of poorly sintered electrodes. Finally and most notably, the regions of performance overlap between the well sintered and poorly sintered cases suggests geometric similarity between microstructures that motivates the development of non-dimensional parameters and scaling relations that can describe electrode performance.

The geometric similarity between microstructures described by the electrochemical fin model was initially explored as a function of the resistivity ratio. As noted, forms of this parameter have been previously introduced in the literature [3,6]. Behavior of the efficiency and dimensionless base current as functions of the resistivity ratio is shown in Fig. 5. For the single conical fin, a base and tip radii of 2.0 and 1.75 μm were used. For the periodic structures segment lengths of 0.25, 0.5, 1.0, and 2.0 μm were considered, and a tip radius of 1.75 μm was applied with a surface charge transfer resistance of 0.6 Ω cm^{-2} and ionic conductivity of 1 S m^{-1}. However, variation of these values led only to minor variation in the data in the curves shown, which confirmed similarity based on geometry. The efficiency accounts for ohmic losses incurred along the length of the extended structure. While it is common to consider the addition of electrode material as generally beneficial to reducing polarization resistance [2,9], this term highlights the trade-off between charge transfer and the ohmic losses incurred by the addition of material and increased constriction in structures with variations in the microstructural cross-section. The behavior of the efficiency as a function of the resistivity ratio reflects this trade-off (Fig. 5a). Here increased ohmic resistance in the solid phase, either through constrictions or the addition of material beyond the active length of the electrode, can result in a less efficient supply of ions to the active surfaces participating in charge transfer. Conversely, the dimensionless base current reflects the benefits of extending the active electrode beyond the electrode–electrolyte plane. The increased active area can lead to increased charge transfer from the electrode, which results in a reduced polarization resistance (Fig. 5b). Variations in the active area for the different geometries considered demonstrate the importance of accounting for detailed microstructural geometry when predicting electrode performance. In the context of the experimental results shown in Fig. 4, the structures with periodic geometry tend to have greater resistivity ratios than the cylindrical geometry, which essentially results from increased surface area per unit volume. These higher resistivity ratios correlate with an increase in the dimensionless base current, which manifests as a reduced polarization resistance in some cases (i.e., well sintered electrodes in general and possibly very thin poorly sintered electrodes).

As is clearly evident from the poorly sintered electrodes shown in Fig. 4, gains in active surface area will not invariably benefit performance. An expense is incurred in terms of ohmic losses that result from the addition of material and the constriction of ionic conduction within the solid phase. This inherent trade-off can be visualized by following the lead of Costamagna et al. [3] and exploring model predictions over a broad range of resistivity ratios, as shown in Fig. 6. Here, a set of periodic geometries are considered using segments with a common base radius of 2 μm and three tip radii 0.25, 0.75, and 1.75 μm. A segment length of 0.25 μm was applied, and total length and ionic conductivity were varied to produce the desired range of resistivity ratios. For the range of resistivity ratios considered the competing ohmic losses and charge transfers gains that occur with increasing resistivity ratio can be seen in the opposing general trends of the efficiency and dimensionless base current. Similar trends may be produced for other dependent variables. For example, the effectiveness can be related to the efficiency through appropriate conversion based on known fin geometry, as implied by Eqs. (26) and (27). For the well sintered (r_t = 1.75 μm) and marginal case (r_t = 0.75 μm) the efficiency behavior is comparable. However, for the case with the smallest tip radius, there is a marked difference. For all three geometries there is substantial difference in the dimensionless base current. This suggests that sintering quality might exert a greater influence over this latter performance metric.

Looking beyond the general trends, several other key insights can be made about the dependence of the efficiency and dimensionless base current on the resistivity ratio. As indicated by the regions marked with Roman numerals, three distinct regimes of transport can be identified. The first of these regimes (I) is designated by $\rho_{io}/\rho_{ct} < 0.1$, analogous to the traditional Biot's number limit for the dominance of convection over conduction heat transfer, and is marked by the dominance of charge transfer behavior with minimal ohmic losses resulting in a high efficiency. In this transport regime performance may not be optimal because not enough additional surface area is added to take full advantage of the charge transfer gains that could be achieved before incurring excessive ohmic penalties. Here, resistance to surface charge transfer results in a low base current (i.e., a high polarization resistance). A constant potential in the electrode structure can be expected for such geometries. In the second regime (II, from $0.1 < \rho_{io}/\rho_{ct} < 10$) a bal-

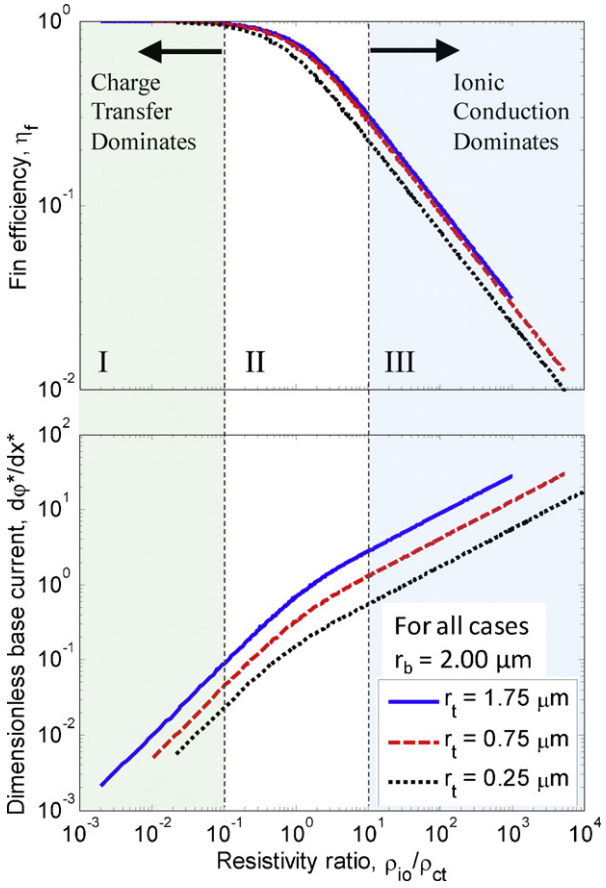

Fig. 6. Fin efficiency (top) and dimensionless base current (bottom) exhibit three regimes of behavior defined on the resistivity ratio. In regime I charge transfer dominates, and low ohmic losses result in high efficiency. In regime II charge transfer and ionic conduction processes are balanced, and electrode performance is best predicted using models that fully account for both processes. In regime III ionic conduction dominates, and electrode performance can be predicted using basic power–law correlations. Performance variations between geometries can be distinguished using the sintering quality.

ance between the charge transfer and ionic conduction is achieved. Electrodes within this region have thickness values that are close to previously defined active lengths for SOFC electrodes [11,13]. Since losses are balanced, geometries suitable for optimum active electrode layers would likely be found in this transitional transport regime. The third regime (III) occurs for $\rho_{io}/\rho_{ct} > 10$ and is marked by the dominance of ionic conduction and ohmic losses over transport. Typically, thicknesses representative of support electrodes fall into this transport regime [23–25]. Since the effects of charge transfer resistance in this regime are reduced, base current values tend to be higher in this regime. However, focusing on regimes II and III a shift to a smaller upward slope for the base current can be seen to coincide with a steeper descent in the efficiency. Particularly for regime III, the rate of decline in performance associated with ohmic losses can be seen to outstrip the rate of gain in performance associated with overall surface charge transfer. Recalling the comparison to Kenjo et al. (Fig. 4), the poorly sintered geometries fall in regime III for a majority of the thickness values investigated (approximately 10–60 μm), whereas the well sintered and cylindrical geometries can be classified as either regimes I or II for thickness up to 40 μm for the variable cross-section case and up to 50 μm for the constant cross-section case. From a charge transport perspective, too much material has been added to electrodes operating in regime III. Charge transfer has passed its maximum limit for the given microstructural geometry, and additional inactive material only adds to ohmic losses. For this regime, addition material provides primarily structural support.

The behavior for the distinct tip geometries applied to obtain the results shown in Fig. 6 reveals the influence of the sintering quality on predicted electrode performance. For the cases shown, the sintering quality (SQ) increases with the tip radius. In terms of both the efficiency and the dimensionless base current a higher sintering quality, indicated by a smaller change in cross-sectional area across the solid structure, results in superior performance. That is, better connectivity among individual elements comprising the periodic structures improves the movement of charge through the solid structure to the active surfaces which produces higher efficiency and lower polarization resistance.

In the regime dominated by ionic conduction (III), linear behavior on the logarithmic scale suggests that a power–law correlation may adequately describe electrode performance in terms of both the resistivity ratio and sintering quality. The cases shown in Fig. 6 were therefore expanded to include geometries with segment lengths of 0.5, 1.0, and 2.0 μm, and a broader set of studies were performed in further pursuit of such a correlation. The set of calculated resistivity ratios, sintering qualities, efficiencies, and dimensionless base currents for the well sintered and marginally sintered cases were transformed to a logarithmic basis and the resulting data were fit to a general linear model. The resulting correlations, inclusive of approximate coefficients and exponents, are shown in Eqs. (30) and (31). Correlation coefficients (R^2) are displayed along with each of these equations. The poorly sintered case was withheld from the correlation process at this point in deference to the more qualitative nature of predictions based on the one-dimensional model for poorly sintered microstructures.

$$\eta_f = \left(\frac{\rho_{io}}{\rho_{ct}}\right)^{-0.49} SQ^{0.02}; \quad R^2 = 0.99 \tag{30}$$

$$\left.\frac{d\varphi^*}{dx^*}\right|_{x^*=0} = 1.5\left(\frac{\rho_{io}}{\rho_{ct}}\right)^{0.55} SQ^{0.25}; \quad R^2 = 0.89 \tag{31}$$

Several points arise from inspection of these correlations, the first being that the physical properties play a dominant role in performance via the resistivity ratio. The trade-off between ohmic and charge transfer losses is again evident in the correlations above as indicated by the reversal of signs on the exponent in the dominant term, and can be further illustrated by observing the behavior of the efficiency and dimensionless base current in terms of the sintering quality, as shown in Fig. 7. Of particular note in these correlations and in Fig. 7 is that the sintering quality has almost negligible influence on efficiency, with microstructural geometry effects largely accounted for in the ratio of the surface area spatial variation (dA_s/dx) and cross sectional area. The sintering quality only exerts influence for poorly sintered structures. On the other hand, the dimensionless base current, which determines the performance gained from adding an extended structure to an active interface, shows a stronger sintering quality influence. This influence demonstrates that adding a poorly sintered structure to an active interface results in less effective electrode for charge transfer.

Further insight into the roles of the resistivity ratio and sintering quality can be gained by considering the exponents applied to the resistivity ratio and sintering quality terms in Eqs. (30) and (31). These exponents take very distinct forms, particularly the approximate square root behavior of the resistivity ratio. Exact square root dependences on the resistivity ratio can be demonstrated analytically by recasting Eq. (20) in terms of the sintering quality and resistivity ratio, as shown in Eq. (32). This ordinary differential equation has the general solution shown in Eq. (33) with α_1 and α_2 defined as the roots of the characteristic equation (Eq. (34)). The constants C_1 and C_2 can be found by applying the appropriate

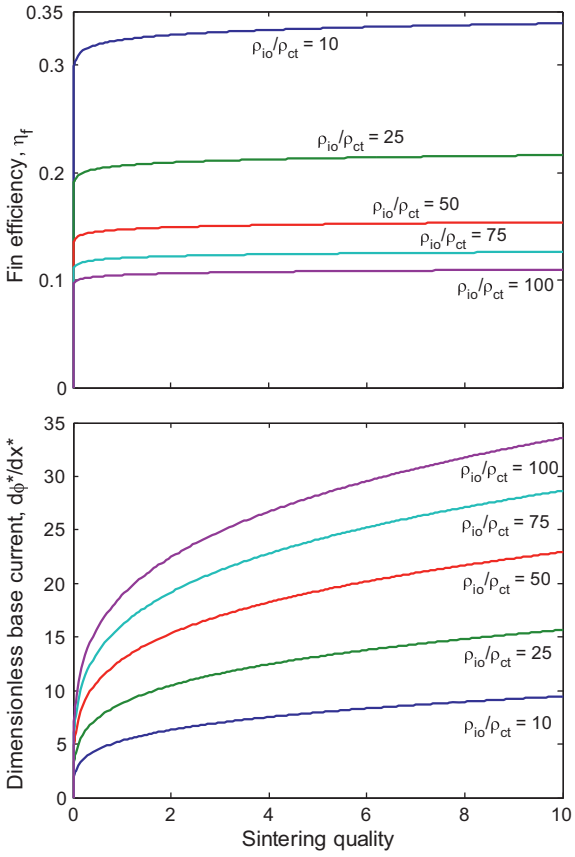

Fig. 7. Power–law predictions of electrode performance in regime III further demonstrate the impact of sintering quality. Efficiency and dimensionless base current increase as sintering quality improves. The latter of these two increases indicates a reduction in polarization resistance.

boundary conditions.

$$\frac{d^2\varphi^*}{dx^{*2}} + \frac{1}{SQ}\frac{d\varphi^*}{dx^*} - \frac{\rho_{io}}{\rho_{ct}}\varphi^* = 0 \tag{32}$$

$$\varphi^*(x^*) = C_1\ \exp(\alpha_1 x^*) + C_2\ \exp(\alpha_2 x^*) \tag{33}$$

$$\alpha_{1,2} = \frac{1}{2}\left[-\frac{1}{SQ} \pm \sqrt{\frac{1}{SQ^2} + 4\left(\frac{\rho_{io}}{\rho_{ct}}\right)}\right] \tag{34}$$

Retaining the general form of the solution for simplicity, the dimensionless base current can be defined in terms of the roots of the characteristic equation, Eq. (35). Furthermore, the efficiency defined in Eq. (26) can be recast in terms of the dimensionless base current, as shown in Eq. (36). It can be seen from Eqs. (34) and (35) that for a well sintered structure (i.e., high sintering quality) the dimensionless base current will reduce to a form proportional to the square root of the resistivity ratio. For the efficiency, inspection of the coefficient on the right hand side of Eq. (36) reveals that it is a close approximation of the inverse of the resistivity ratio. Multiplication of the dimensionless current by this term leads to the inverse square root dependence and further reduction of the sintering quality's influence on the efficiency, both seen in Eq. (30). Since the structures considered for the correlations above retain some variation in cross-sectional geometry, the sintering quality still exerts some influence in both correlations, even when ionic conduction is dominant and power law behavior is observed. This demonstration of the exact square root dependence confirms the trends revealed by the power law correlations for electrode performance in regime III. However, more importantly, it also provides forms of the dimensionless base current and efficiency that allow for rapid assessment of electrode performance in all of the transport regimes indicated in Fig. 6.

$$\left.\frac{d\varphi^*}{dx^*}\right|_{x^*=0} = C_1\alpha_1 + C_2\alpha_2 \tag{35}$$

$$\eta_f = \frac{\sigma_{io}R_{ct}A_b}{L_fA_f}\left.\frac{d\varphi^*}{dx^*}\right|_{x^*=0} \tag{36}$$

A final insight that comes from the role of the resistivity ratio relates to the size of the active region within the SOFC electrode. Considering the parameter m defined in Eq. (11), an active length can be defined for the electrochemical fin that is analogous to the healing length of a thermal fin, Eq. (37). Similar active lengths have been defined for SOFC electrodes in the literature [11,13]. Note that the perimeter defines the spatial variation in surface area for the special case of a constant cross-section fin and has been generalized in Eq. (37). The resistivity ratio can then be expressed in terms of the active length and total electrode thickness, as shown in Eq. (38). Thus, it can be seen that both the efficiency and dimensionless base current scale primarily in terms of the ratio of active length to total electrode thickness. If the total thickness exceeds the active length, a penalty is extracted through higher ohmic loss incurred by excess material. However, the addition of material can enhance the charge transfer capabilities of the electrode, which reduces the total polarization resistance.

$$L_{act} = \frac{1}{m} = \left[\frac{1}{\sigma_{io}R_{ct}}\frac{1}{A_c}\frac{dA_s}{dx}\right]^{-1/2} \tag{37}$$

$$\frac{\rho_{io}}{\rho_{ct}} = \frac{L_f^2}{L_{act}^2} \tag{38}$$

As noted, the trends in Fig. 6 contain an inflection point near the active length defined above. The addition of material beyond this length leads to a greater dominance of ohmic losses associated with ionic transport because the inactive material increases resistance. However, such material may fulfill a vital structural support role. The active length provides a demarcation for transitioning microstructural design objectives from a transport and electrochemistry perspective to a structural support perspective.

4. Conclusions

An extended surface modeling concept (the electrochemical fin) has been applied to explore charge transport within SOFC electrodes using an analytical modeling approach. This model represents an advance from existing thin film models in terms of the phase of interest and the application of a variable cross-section equation that enables the analytical exploration of the role of microstructure on performance. Parallels between the model presented and the thin film approach are strong enough to warrant cognizance of thin film model critiques that may apply. The present work attempts to address one such issue, connectivity of the ionic conducting phase, through consideration variable cross-section geometry in solid structures. Drawing from this approach the model presented is capable of replicating experimentally observed electrode behavior inclusive of sensitivity to microstructural geometry associated with sintering without relying on effective conductivity parameters. This capability stands in contrast to similar models that rely on a constant cross-section formalism in the governing equation.

One-dimensional models have been explored for electrochemical fins of several cross-sectional geometries, providing the foundation for a general tool that enables prompt performance evaluation of electrode microstructures and facilitates SOFC microstructural design by focusing more detailed modeling efforts on the most promising microstructures. Insights garnered

from these explorations include: the establishment of a suite of dimensionless parameters and performance metrics that can be applied to assess electrode microstructure, the definition of microstructure-related transport regimes relevant to electrode design, and correlations that allow performance predictions for electrodes that also provide cell structural support. Of particular note, the model developed motivates the definition of a novel sintering quality parameter that quantifies the degree of constriction within the conducting network of the electrode, which may influence electrode polarization. While many key insights can be gained from these developments, further exploration of microstructural geometry is needed to achieve more general applicability of the electrochemical fin approach to transport in SOFC electrodes. These explorations include the addition of space charge effects, consideration the role of multi-dimensional transport, and connection of the modeling approach presented to real electrode microstructures.

Acknowledgements

Financial support from an Energy Frontier Research Center on Science Based Nano-Structure Design and Synthesis of Heterogeneous Functional Materials for Energy Systems (HeteroFoaM Center) funded by the U.S. Department of Energy, Office of Science, Office of Basic Energy Sciences (Award DE-SC0001061) is gratefully acknowledged. The authors are grateful to Prof. Anil V. Virkar at the University of Utah and Prof. Brice N. Cassenti at the University of Connecticut for invaluable discussions on SOFC microstructure and analytical solution methods, respectively.

References

[1] K. Reifsnider, X. Huang, G. Ju, R. Solasi, Journal of Material Science 41 (2006) 6751–6759.
[2] C.W. Tanner, K. Fung, A.V. Virkar, Journal of the Electrochemical Society 144 (1997) 21–30.
[3] P. Costamagna, P. Costa, V. Antonucci, Electrochimica Acta 43 (1998) 375–394.
[4] H. Zhu, R.J. Kee, Journal of the Electrochemical Society 155 (2008) B715–B729.
[5] M. Cannarozzo, S. Grosso, G. Agnew, A. Del Borghi, P. Costamagna, Journal of Fuel Cell Science and Technology 4 (2007) 99–106.
[6] S. Sunde, Journal of Electroceramics 5 (2000) 153–182.
[7] S. Sunde, Journal of the Electrochemical Society 143 (1996) 1123–1133.
[8] S. Sunde, Journal of the Electrochemical Society 143 (1996) 1930–1939.
[9] T. Kenjo, S. Osawa, K. Fujikawa, Journal of the Electrochemical Society 138 (1991) 349–355.
[10] T. Kenjo, M. Nishiya, Solid State Ionics 57 (1992) 295–302.
[11] P. Costamagna, P. Costa, E. Arato, Electrochimica Acta 43 (1998) 967–972.
[12] J. Fleig, J. Maier, Journal of the European Ceramic Society 24 (2004) 1343–1347.
[13] M. Liu, Journal of the Electrochemical Society 145 (1998) 142–154.
[14] J.H. Nam, D.H. Jeon, Electrochimica Acta 51 (2006) 3446–3460.
[15] L.C.R. Schneider, C.L. Martin, Y. Bultel, D. Bouvard, E. Siebert, Electrochimica Acta 52 (2006) 314–324.
[16] L.C.R. Schneider, C.L. Martin, Y. Bultel, L. Dessemond, D. Bouvard, Electrochimica Acta 52 (2007) 3190–3198.
[17] F. Zhao, A.V. Virkar, Journal of Power Sources 195 (2010) 6268–6279.
[18] J.R. Izzo Jr., A.S. Joshi, K.N. Grew, W.K.S. Chiu, A. Tkachuk, S.H. Wang, W. Yun, Journal of the Electrochemical Society 155 (2008) B504–B508.
[19] K.N. Grew, Y.S. Chu, J. Yi, A.A. Peracchio, J.R. Izzo Jr., Y. Hwu, F. De Carlo, W.K.S. Chiu, Journal of the Electrochemical Society 157 (2010) B783–B792.
[20] J.R. Wilson, W. Kobsiriphat, R. Mendoza, H. Chen, J.M. Hiller, D.J. Miller, K. Thornton, P.W. Voorhees, S.B. Adler, S.A. Barnett, Nature Materials 5 (2006) 541–544.
[21] A. Faes, A. Hessler-Wyser, D. Presvytes, C.G. Vayenas, J. Vanherle, Fuel Cells 9 (2009) 841–851.
[22] P. Tanasini, M. Cannarozzo, P. Costamagna, A. Faes, J. Van Herle, A. Hessler-Wyser, C. Comninellis, Fuel Cells 9 (2009) 740–752.
[23] B.W. Chung, C.N. Chervin, J.J. Haslam, A. Pham, R.S. Glassa, Journal of the Electrochemical Society 152 (2005) A265–A269.
[24] J. Kim, A.V. Virkar, K. Fung, K. Mehta, S.C. Singhal, Journal of the Electrochemical Society 146 (1999) 69–78.
[25] F. Zhao, A.V. Virkar, Journal of Power Sources 141 (2005) 79–95.